GEOLOGY | THE GEOLOGICAL SOCIETY OF AMERICA®

https://doi.org/10.1130/G53096.1

Manuscript received 6 January 2025
Manuscript accepted 3 March 2025

Published online 12 March 2025

Crater-wall degradation and bedrock-chute formation from dry rockfall erosion

Benjamin T. Cardenas[1], Alexander R. Beer[2], Patrick J. Donohoe[3], Oak Kanine[3], James L. Dickson[4], and Michael P. Lamb[3,*]

[1]Department of Geosciences, The Pennsylvania State University, University Park, Pennsylvania 16802, USA
[2]Department of Geosciences, University of Tübingen, D-72076 Tübingen, Germany
[3]Division of Geological and Planetary Sciences, California Institute of Technology, Pasadena, California 91125, USA
[4]Department of Earth and Environmental Sciences, Polar Geospatial Center, University of Minnesota, Saint Paul, Minnesota 55108, USA

ABSTRACT

Impact cratering is a key process on rocky bodies in the solar system. The subsequent degradation of impact-crater walls can record ancient environmental conditions, such as surface water on Mars. Distinguishing erosional landforms associated with liquids from those associated with dry processes remains challenging. Here, we developed a model for landform development under a dry end-member case of degradation by rockfall. Unlike canonical models of crater degradation by regolith creep that smooth and relax hillslopes, results show that rockfalls produce channelized landforms. Rockfall locally oversteepens slopes, leading to increased rockfall generation, which is then funneled into topographic lows, causing chute development through topographic feedback similar to river incision. While typically neglected in landscape evolution models, rockfalls can shape crater walls and steep rocky slopes, creating channelized landforms by dry processes that are not possible with regolith creep alone.

INTRODUCTION

Impact cratering is a dominant process on rocky planets and moons (Fig. 1; Hartmann, 1972; Fassett, 2016). Postimpact crater degradation is equally important because it can record information about the type, pace, and history of erosional processes driven by wind, water, or volatile activity and disturbance-driven regolith creep (Garvin and Frawley, 1998; Craddock and Howard, 2000). Many models of crater degradation have focused on regolith creep, which manifests as topographic diffusion (Craddock and Howard, 2000; Fassett and Thomson, 2014), producing crater walls that smooth over time. However, some old crater walls are not smooth (Levin et al., 2022; Sun et al., 2022). On Mars and Earth, deviations from smooth walls—such as rocky spurs and chutes (Fig. 1)—have been attributed to erosional processes related to water, including fluvial incision (Howard, 2007; Kumar et al., 2010; Bamber et al., 2022), debris flows, groundwater sapping (Malin and Edgett, 2000; Salese et al., 2019), or other volatiles (Conway et al., 2018). Dry erosional processes have also likely shaped steep terrain on Earth, even in relatively humid conditions (Hsu et al., 2008; DiBiase et al., 2017). Likewise, they have contributed to the formation of gullies in regolith on Mars (Pilorget and Forget, 2016; Conway et al., 2019) and are likely the cause for chutes on the Moon (Kokelaar et al., 2017) and Mercury (Fassett et al., 2017; Malliband et al., 2019), but the roles of different erosional processes, substrates, and volatiles in chute formation remain debated.

Recent work has emphasized the importance of a lithified substrate in bedrock-chute formation by dry rockfall, where the strong substrate allows channelized landforms with tens of meters of relief (Levin et al., 2022) to persist through multiple rockfall events (Sun et al., 2022; Beer et al., 2024). Through topographic feedback, similar to river incision, the rockfall is funneled into proto-chutes, leading to preferential abrasion of the chute floor and further chute development (Sun et al., 2022). On Mars, volatiles are thought to have played some role in bedrock-chute formation, at least at higher latitudes, due to correlations between chute formation, latitude, and slope aspect (Levin et al., 2022), though the drivers of rockfall vary across the planet (Bickel et al., 2024). Rockfall could be a dominant process in bedrock-chute formation at low latitudes on Mars and on the Moon and other rocky planets and moons (Levin et al., 2022), but it remains poorly understood.

Here, we developed a novel landscape evolution model for crater-wall degradation by regolith creep and rockfall erosion. We purposefully neglected fluvial incision to investigate whether dry processes alone can produce the observed crater-wall morphologies. Regolith creep is likely important in crater degradation, but it cannot explain the spurs and chutes common in rocky craters (Fig. 1; e.g., Levin et al., 2022). Therefore, we included bedrock erosion driven by impacts from rockfall, utilizing a recent mechanistic theory (Beer et al., 2024). Many models of granular flows and avalanches exist (Savage, 1979; Howard, 1998), but these are intended for granular substrates, rather than bedrock erosion, and create lobate topography at the grain scale (e.g., Félix and Thomas, 2004), not chutes with tens of meters of relief (Levin et al., 2022).

METHODS

Our modeled scenario (Fig. 2A) used an initial crater topography for a simple, 1-km-diameter, 260-m-deep bedrock impact crater, following Howard (2007). The topography was laid out on a cartesian grid with 2 m × 2 m cells, and we modeled one quarter of the crater for computational efficiency. The model solved for the change in elevation in time as $\frac{\partial z}{\partial t} = -D\nabla^2 z + E_r$ in the Landlab landscape evolution framework (Hobley et al., 2017; Barnhart et al., 2020). The first term on the right-hand side represents topo-

Benjamin T. Cardenas https://orcid.org/0000-0001-7246-219X
Michael P. Lamb https://orcid.org/0000-0002-5701-0504
*mpl@caltech.edu

CITATION: Cardenas, B.T., et al., 2025, Crater-wall degradation and bedrock-chute formation from dry rockfall erosion: Geology, v. 53, p. 456–460, https://doi.org/10.1130/G53096.1

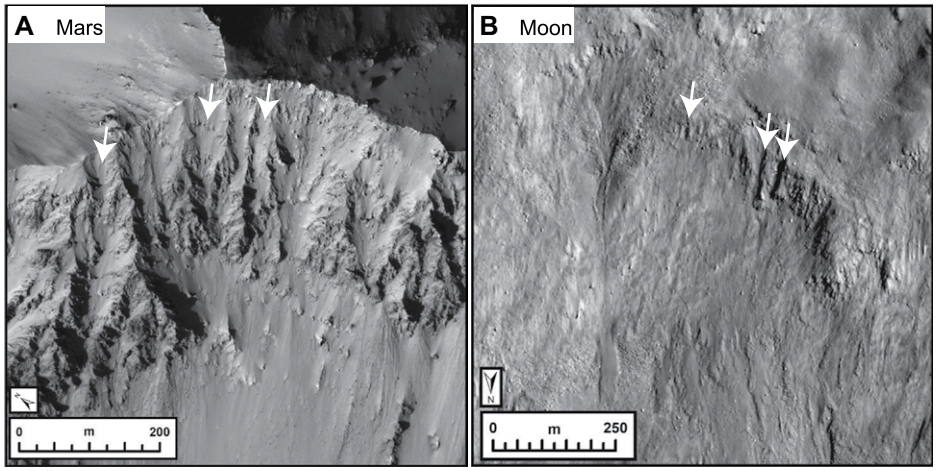

Figure 1. Crater-wall bedrock chutes on (A) Mars at 77.34°E, 21.18°S (credit: National Aeronautics and Space Administration [NASA]/Jet Propulsion Laboratory/University of Arizona) and (B) the Moon at −46.04°E, 12.37°N (credit: NASA/Goddard Space Flight Center/Arizona State University). Arrows point to tops of chutes.

graphic diffusion from linear slope-dependent creep, where D [L^2/T] is the diffusivity. The second term represents the rockfall erosion rate, given by $E_r = \Sigma\delta/\Delta t$, where δ is the bedrock erosion per impact, summed over the number of impacts at a given grid cell in a given time step, Δt. To model rockfall erosion, we used the model of Beer et al. (2024), which tracks individual rockfall trajectories using the physics of ballistic trajectories, and it relates bedrock erosion to rockfall impact kinetic energy and bedrock tensile strength (Beer et al., 2024). The model was tested and calibrated against laboratory experiments and explicitly includes gravity, so that it can be adapted to Mars (Beer et al., 2024). See Supplemental Material Text S1[1] and Beer et al. (2024) for the model details.

During each time step, we tracked the ballistic trajectory of 100 grains with diameter = 0.25 m and calculated their contribution to erosion, $\Sigma\delta$, from Beer et al. (2024). This uniform diameter was selected as a compromise between subpixel resolution and erosion per impact. Rockfall frequency was determined by $f = n_r/t_r$, in which n_r is the number of rockfall events that occurs within a representative time span, t_r. We assumed that n_r scales with the number of oversteepened cells capable of generating rockfall, n_s, such that $n_r = cn_s$. An oversteepened cell has a slope greater than a threshold, $-\nabla z > S_c$, which we set to $S_c = 1$ (i.e., 45°; e.g., DiBiase et al., 2017). Thus, $f = cn_s/t_r$, and the model produces more frequent rockfall events when the topography has a larger rockfall source area. Each rockfall source location was picked randomly from a uniform distribution of the n_s possible source locations. We updated the topography resulting from impact erosion and topographic diffusion (solved using a Landlab tool) after every 100 rockfall events, and so we used a variable time step such that $\Delta t = 100/f$. Under this criterion, $\Delta t = \frac{100}{f} = \frac{100t_r}{cn_s}$. We set $t_r/c = 1$ k.y. as an arbitrary estimate that yielded bedrock-chute topography given the assumed rates of regolith creep (see below).

We roughened the initial topography by adding topographic noise of 0–2 m elevation per cell from a uniform distribution. This generated slopes greater than 45° for 5.77% of cells ($n_s = 3958$), which became the initial rockfall source locations. The elevations at the rockfall starting and stopping cells were raised and lowered by the rockfall volume normalized by the cell area. Rockfall talus was treated as having the same erosional properties as bedrock for simplicity. We ran nine experiments, each beginning with the same roughened topography and running for 1.9 million model years (m.y.), which was enough time to develop bedrock chutes. Given our model assumptions, it is unknown if this time frame is representative. In each experiment, we varied D by a large exploratory range from $D = 10^{-9}$ m^2/yr to $D = 10^{-1}$ m^2/yr. Values between 10^{-9} m^2/yr and 10^{-4} m^2/yr have been inferred for Mars (Howard, 2007; Golombek et al., 2014).

We extracted elevations along concentric transects at 10 m intervals from the crater's center, after Levin et al. (2022), every 5 k.y. We smoothed each transect with a 6 m rolling average to reduce noise and calculated chute width, depth, and the width-depth ratio along these transects. We defined chute depth as the relief between a local trough and the adjacent peak, and we defined width as twice the horizontal distance between the trough and peak. To assess the contribution of rockfall and regolith creep to total erosion, we saved the erosion from each process every 5 k.y. The model and all data can be found in Cardenas et al. (2023).

RESULTS

Experiments with diffusivities of $D = 10^{-5}$ m^2/yr and higher smoothed the topography and lowered the local slopes, eliminating rockfall events within several thousand years. These experiments did not produce chutes. Here, we focus on experiments that did produce chutes, comparing results from a low-diffusivity case (experiment 1; $D = 10^{-9}$ m^2/yr) and a high-diffusivity case (experiment 2; $D = 10^{-6}$ m^2/yr).

Unlike simulations dominated by regolith creep ($D > 10^{-5}$ m^2/yr), experiments with more moderate rates of regolith creep produced bedrock chutes with relief of several meters (Figs. 2B–2C). Chutes developed across the crater wall, merging and splitting over time (Figs. 2B–2C). The crater wall steepened in time, as seen in longitudinal profiles (Fig. 2D). The initial crater wall averaged 24°, while along-chute profiles averaged 30° (experiment 1) and 38° (experiment 2). Shallower aprons near the bottom of the crater walls were resting locations of rocks, most of which did not reach farther into the crater center by the end (Figs. 2B–2C).

In experiment 1, which had negligible regolith creep ($D = 10^{-9}$ m^2/yr), we measured 2616 chute cross sections along the concentric topographic transects by 1.9 m.y. From these cross sections, the median chute width was 16.49 m, depth was 4.09 m, and width-depth ratio was 3.91. In experiment 2, with greater regolith creep ($D = 10^{-6}$ m^2/yr), the number of chute cross sections was lower by 16% (2197) at the same time (1.9 m.y.). Median chute width was 20.4 m, depth was 4.4 m, and width-depth ratio was 4.7. The distributions appear comparable between the two experiments (Figs. 3A–3C), but a two-sample Kolmogorov-Smirnov test rejected their similarity. Depths were closest to similar ($p = 0.003$), suggesting diffusivity had less influence on depths and more on widths, and thus width-depth ratios. The higher diffusivity in experiment 2 drove faster outward migration of chute walls. However, the contribution of regolith creep to total crater erosion by volume was overall small, at 10^{-8}% for experiment 1 and 10^{-5}% for experiment 2.

Over time, both experiments showed increases in chute width and depth and decreases in the width-depth ratio (Figs. 3D–3F). After 0.5 m.y., experiment 2 had a deeper median chute, though by only a few tens of centimeters (Fig. 3E). After 1 m.y., experiment 2 had a median chute width 3 m greater than experiment 1 (Fig. 3D). The width-depth ratio varied by ~2 for both experiments from 0.5 m.y. until

[1]Supplemental Material. A full description of the rockfall model used in this manuscript. Please visit https://doi.org/10.1130/GEOL.S.28543637 to access the supplemental material; contact editing@geosociety.org with any questions.

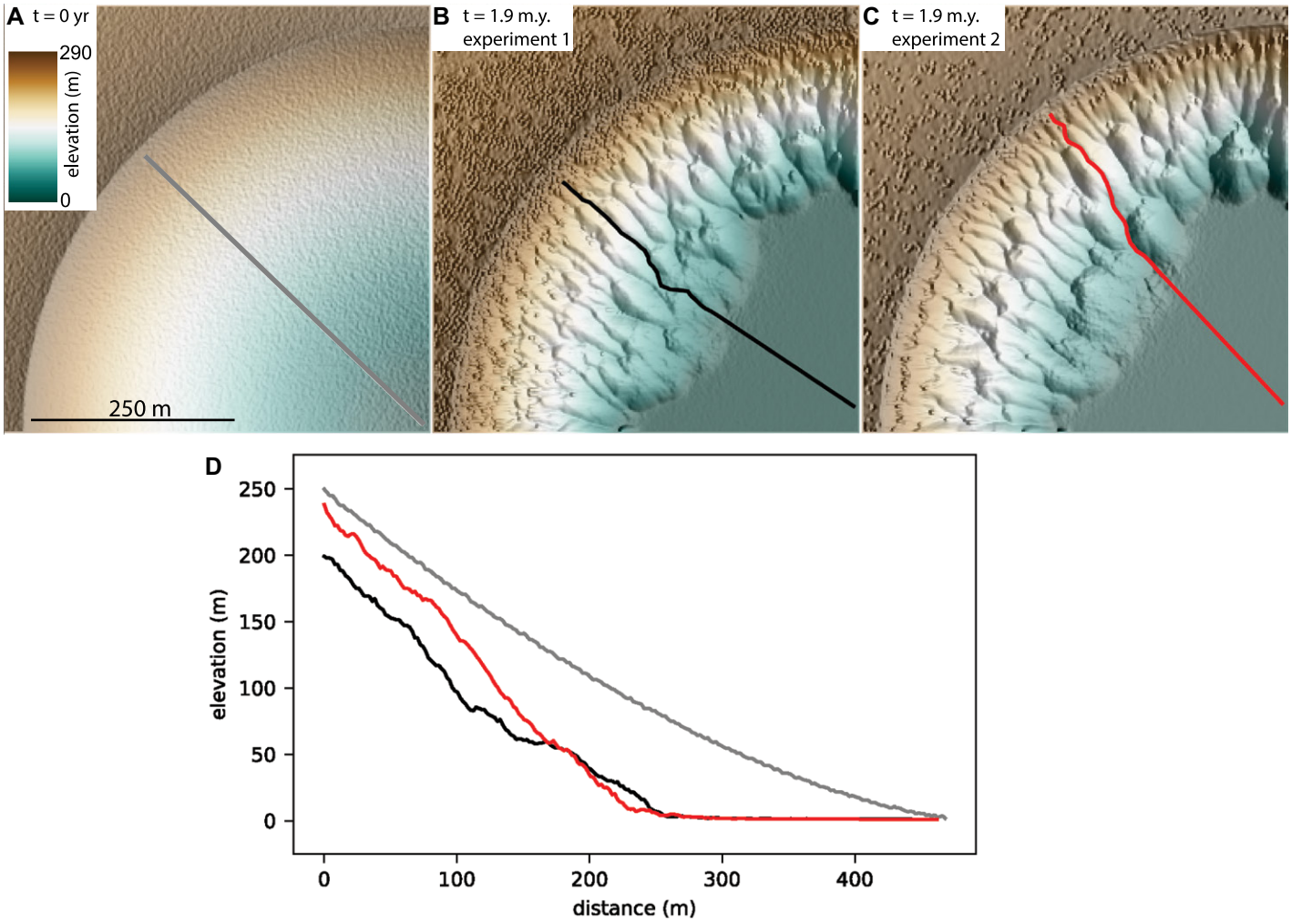

Figure 2. Hillshade maps showing initial and evolved synthetic crater topography generated during 1.9 m.y. of rockfall and topographic diffusion. Illumination comes from right at 45° angle. Stippling close to crater rim and outside crater is due to initial surface roughening. Downslope lines in each panel trace longitudinal profiles shown in panel D. (A) Crater topography at $t = 0$ yr. (B) Experiment 1 at $t = 1.9$ m.y. (C) Experiment 2 at $t = 1.9$ m.y. (D) Long profiles from panels A–C.

the end. Each width-depth ratio curve showed a decrease in the rate of change after $t = 1$ m.y. (Figs. 3D–3F).

Rockfall erosion and chute development increased local topographic slopes and therefore caused the number of rockfall events to increase in time (Fig. 3G). This topographic feedback allowed rockfall erosion to be self-sustaining. Owing to slower regolith creep, experiment 1 developed steeper topography and consistently more rockfall events through time than experiment 2 developed (Fig. 3G). In each experiment, the total volume of eroded material increased more linearly with time as compared to the number of rockfalls (Fig. 3H). The similar total erosion between both experiments, in spite of the greater number of rockfalls in experiment 1, suggests the deeper, narrower chutes developed in experiment 1 were more efficient at funneling rockfalls to the crater floor.

Large bedrock chutes were relatively late-stage landforms in both experiments (Fig. 4). At $t = 0.5$ m.y., the 150 m topographic contour showed erosion, but the chutes were narrow and shallow proto-chutes. At $t = 1$ m.y., chutes were recognizable as upslope-pointing V-shapes in the topographic contours. The largest change in chute size occurred between $t = 1.5$ and 1.9 m.y. (Figs. 4A–4B). Chute growth at the 220 m topographic contour was diminished due to less material being available to funnel into this high-elevation location. Erosion was greatest at the 30 m contour, based on the distance the contour line stepped back with time (Figs. 4A–4B). Both experiments eroded the total crater wall toward the rim by a similar distance at each contour by $t = 1.9$ m.y. (Fig. 4C).

DISCUSSION

Regolith creep creates smooth walls that relax over time. Although this is often considered the dominant process in crater-wall degradation, many rocky slopes on Earth (e.g., Beer et al., 2024) and degraded crater walls on Mars (Levin et al., 2022; Sun et al., 2022), the Moon (Levin et al., 2022), and Mercury (Fassett et al., 2017; Malliband et al., 2019) show rough, chute-and-spur topography. Our simulations illustrate how these landforms can develop by rockfall erosion. A lithified substrate with relatively low rates of regolith creep is likely required, as it allows proto-chutes to persist through multiple rockfall events and to enlarge (Fig. 4), consistent with physical experiments (Sun et al., 2022; Beer et al., 2024). Unlike channelized landforms that form rapidly in granular substrates (Howard, 1998), large bedrock chutes in our simulations took millions of years to develop, potentially recording environmental conditions over that period (Levin et al., 2022).

Although rockfall can be triggered by seismic or volatile activity (Vijayan et al., 2022; Ruj et al., 2022), our model demonstrated self-generated rockfall events, consistent with the variety of conditions associated with rockfall on Mars (Bickel et al., 2024). Rockfall was triggered where the local gradient exceeded 45°, resulting in sustained rockfall over 1.9 m.y. New source locations emerged as the topogra-

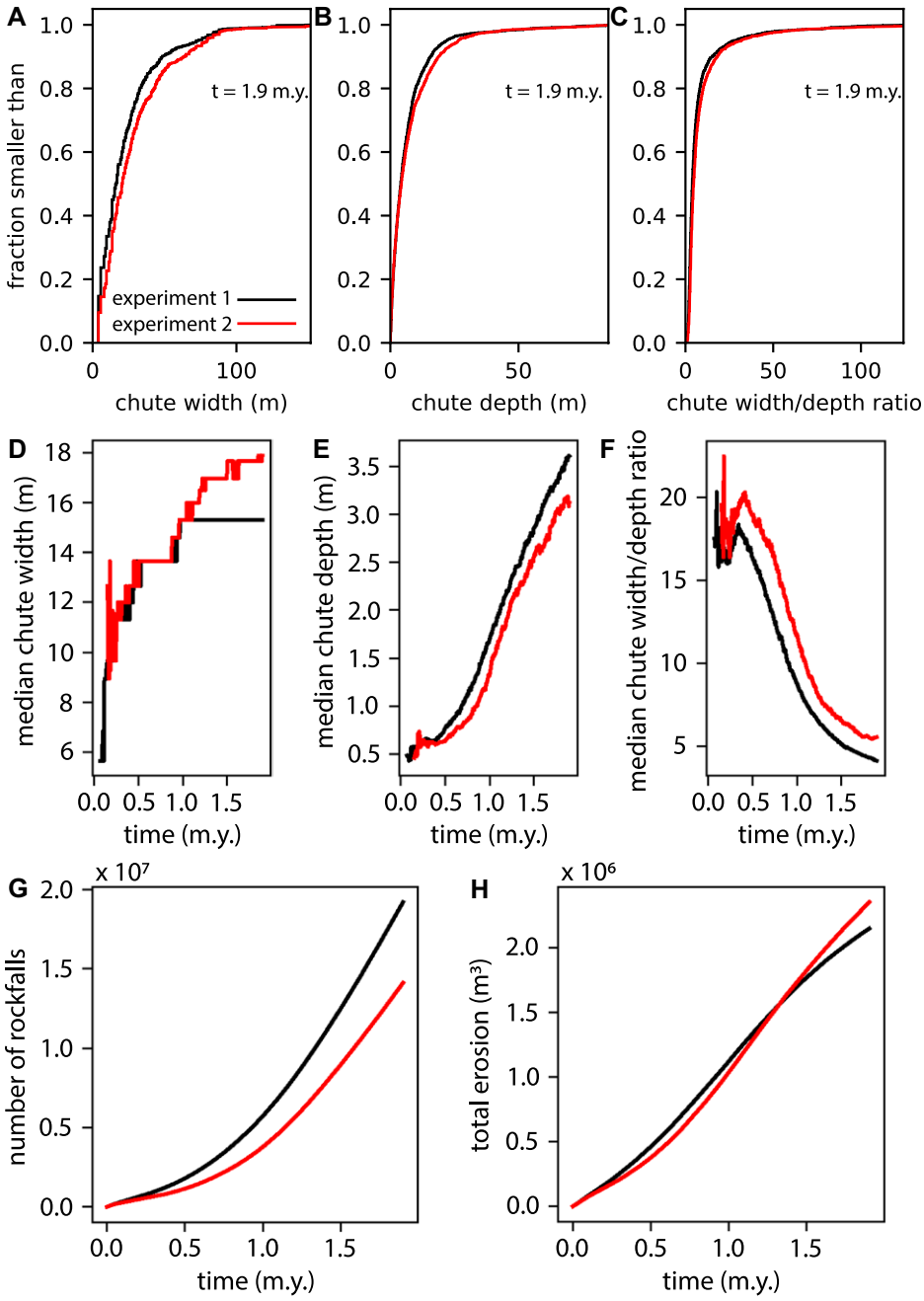

Figure 3. Bedrock chute geometry over time and at t = 1.9 m.y. (A) Cumulative distribution functions (CDFs) of final chute width. (B) CDFs of final chute depth. (C) CDFs showing final width-depth ratios. (D) Time evolution of median chute width. Aliasing is due to 2 m grid size. (E) Evolution of median chute depth. (F) Evolution of median width-depth ratio. (G) Cumulative number of total rockfalls over time. (H) Cumulative volume of eroded material over time.

phy developed, causing a nonlinear increase in rockfall events with time (Fig. 3G). Chute width and depth were still increasing at the end of our simulations at t = 1.9 m.y., with the width-to-depth ratio decreasing (Figs. 3D–3F), suggesting chutes would continue to enlarge and change shape in longer simulations. Though the rate of change slowed after 1 m.y. (Figs. 2D–2F), the chutes did not reach a steady-state geometry. It is unknown if a characteristic chute geometry would emerge, as it does in landscapes shaped by competing erosional processes balanced with uplift (Perron et al., 2008), but eventually, rockfall initiation must cease as crater walls flatten or are buried in talus.

Rockfalls and dry granular avalanches are often considered ineffective for gradients below the angle of repose, typically 30°–45°. For example, the Marathon Valley on Mars was argued to be fluvial due to its 18° longitudinal slope (Grant et al., 2016; Hughes et al., 2019). Chutes in our simulations had average gradients of 30° and 38° in experiments 1 and 2, but with lower gradients on the tail of the distribution. For example, 24% and 15% of the chutes in experiments 1 and 2, respectively, had gradients lower than 18°. Chute development was possible at these lower gradients because large rocks over relatively smooth bedrock topography can run-out to gradients far less than the typical angle of repose (e.g., DiBiase et al., 2017).

Can rockfall chutes be distinguished from channelized landforms produced by water or other volatiles? Some modeled chutes converged downstream (Fig. 2), similar to weakly developed drainage networks. Nonetheless, networks of channels on Mars in low-gradient plains (<∼10°) are unlikely to have formed through dry rockfall. Additionally, given the latitude and orientation controls on Martian chute geometry (Levin et al., 2022), volatiles likely played a role in triggering some rockfall events.

In conclusion, rockfalls can be self-generated on steep, degrading rocky slopes, counteracting topographic smoothing by regolith creep, and creating channelized landforms and chute-and-spur topography even without fluid-driven erosion.

ACKNOWLEDGMENTS

M.P. Lamb acknowledges funding from National Aeronautics and Space Administration grant 80NSSC19K1269. We thank science editor Kathleen Benison for handling our manuscript. E. Bamber, two anonymous scientists, A. Howard, and S. Conway provided helpful reviews.

REFERENCES CITED

Bamber, E.R., Goudge, T.A., Fassett, C.I., and Osinski, G.R., 2022, Constraining the formation of paleolake inlet valleys across crater rims: Icarus, v. 378, https://doi.org/10.1016/j.icarus.2022.114945.

Barnhart, K.R., et al., 2020, Short communication: Landlab v2.0: A software package for Earth surface dynamics: Earth Surface Dynamics, v. 8, p. 379–397, https://doi.org/10.5194/esurf-8-379-2020.

Beer, A.R., Fischer, J.N., Ulizio, T.P., Ma, Z., Sun, Z., and Lamb, M.P., 2024, A mechanistic model and experiments of bedrock incision and channelization by rockfall: Journal of Geophysical Research: Earth Surface, v. 129, no. 3, https://doi.org/10.1029/2023JF007504.

Bickel, V.T., Daubar, I.J., Sokolowska, A.J., Bonab, A., Haut, I., and Conway, S.J., 2024, The first global catalog of rockfall locations on Mars: Geophysical Research Letters, v. 51, no. 24, https://doi.org/10.1029/2024GL110674.

Cardenas, B.T., Beer, A.R., Donohoe, P.J., Kanine, O., Dickson, J.L., and Lamb, M.P., 2023, Model and data for "Crater-wall degradation and bedrock-chute formation from dry rockfall erosion": Scholarsphere, https://doi.org/10.26207/rdex-en91.

Conway, S.J., Butcher, F.E.G., de Haas, T., Deijns, A.A.J., Grindrod, P.M., and Davis, J.M., 2018, Glacial and gully erosion on Mars: A terrestrial perspective: Geomorphology, v. 318, p. 26–57, https://doi.org/10.1016/j.geomorph.2018.05.019.

Conway, S.J., de Haas, T., and Harrison, T.N., 2019, Martian gullies: A comprehensive review of observations, mechanisms and insights from Earth analogues, *in* Conway, S.J., et al., eds., Martian Gullies and their Earth Analogues: Geological Society, London, Special Publication 467, p. 7–66, https://doi.org/10.1144/SP467.14.

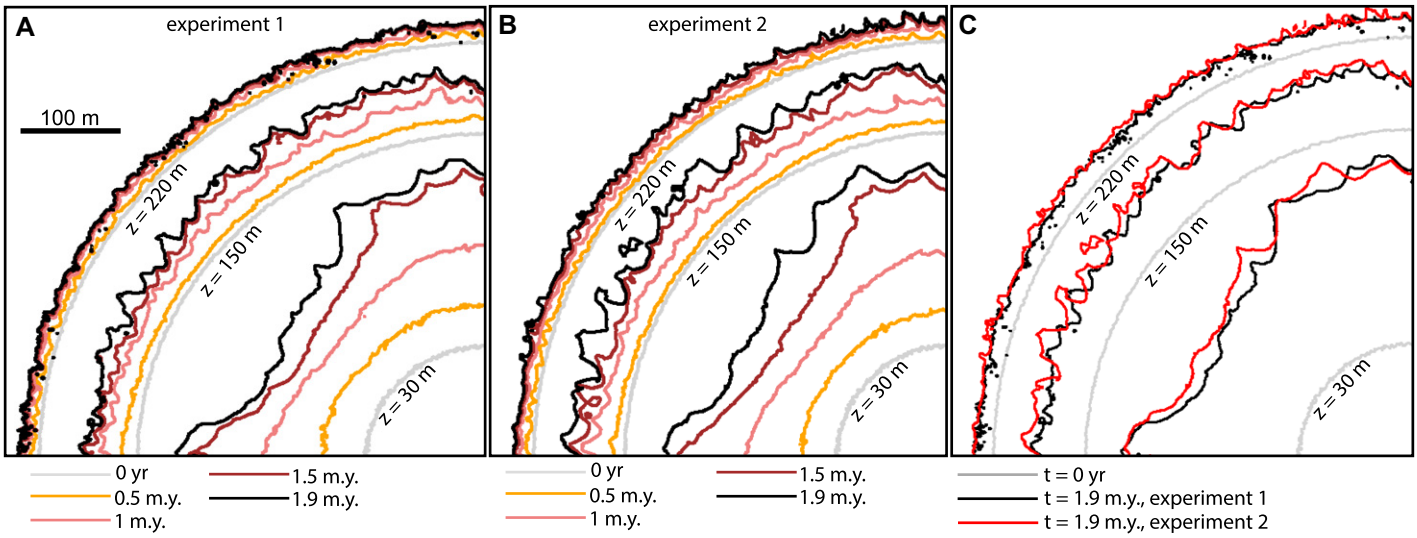

Figure 4. Evolution of topographic contours over time. Each panel shows 30 m, 150 m, and 220 m contours. (A) Evolution of contours in experiment 1. (B) Evolution of contours in experiment 2. (C) Overlain contours at $t = 0$ and $t = 1.9$ m.y. for experiments 1 and 2.

Craddock, R.A., and Howard, A.D., 2000, Simulated degradation of lunar impact craters and a new method for age dating farside mare deposits: Journal of Geophysical Research: Planets, v. 105, p. 20,387–20,401, https://doi.org/10.1029/1999JE001099.

DiBiase, R.A., Lamb, M.P., Ganti, V., and Booth, A.M., 2017, Slope, grain size, and roughness controls on dry sediment transport and storage on steep hillslopes: Particle transport on steep hillslopes: Journal of Geophysical Research: Earth Surface, v. 122, p. 941–960, https://doi.org/10.1002/2016JF003970.

Fassett, C.I., 2016, Analysis of impact crater populations and the geochronology of planetary surfaces in the inner solar system: Journal of Geophysical Research: Planets, v. 121, p. 1900–1926, https://doi.org/10.1002/2016JE005094.

Fassett, C.I., and Thomson, B.J., 2014, Crater degradation on the lunar maria: Topographic diffusion and the rate of erosion on the Moon: Journal of Geophysical Research: Planets, v. 119, p. 2255–2271, https://doi.org/10.1002/2014JE004698.

Fassett, C.I., Crowley, M.C., Leight, C., Dyar, M.D., Minton, D.A., Hirabayashi, M., Thomson, B.J., and Watters, W.A., 2017, Evidence for rapid topographic evolution and crater degradation on Mercury from simple crater morphometry: Geophysical Research Letters, v. 44, p. 5326–5335, https://doi.org/10.1002/2017GL073769.

Félix, G., and Thomas, N., 2004, Relation between dry granular flow regimes and morphology of deposits: Formation of levées in pyroclastic deposits: Earth and Planetary Science Letters, v. 221, p. 197–213, https://doi.org/10.1016/S0012-821X(04)00111-6.

Garvin, J.B., and Frawley, J.J., 1998, Geometric properties of Martian impact craters: Preliminary results from the Mars Orbiter Laser Altimeter: Geophysical Research Letters, v. 25, p. 4405–4408, https://doi.org/10.1029/1998GL900177.

Golombek, M.P., Warner, N.H., Ganti, V., Lamb, M.P., Parker, T.J., Fergason, R.L., and Sullivan, R., 2014, Small crater modification on Meridiani Planum and implications for erosion rates and climate change on Mars: Journal of Geophysical Research: Planets, v. 119, p. 2522–2547, https://doi.org/10.1002/2014JE004658.

Grant, J.A., Parker, T.J., Crumpler, L.S., Wilson, S.A., Golombek, M.P., and Mittlefehldt, D.W., 2016, The degradational history of Endeavour crater, Mars: Icarus, v. 280, p. 22–36, https://doi.org/10.1016/j.icarus.2015.08.019.

Hartmann, W.K., 1972, Paleocratering of the Moon: Review of post-*Apollo* data: Astrophysics and Space Science, v. 17, p. 48–64, https://doi.org/10.1007/BF00642541.

Hobley, D.E.J., Adams, J.M., Nudurupati, S.S., Hutton, E.W.H., Gasparini, N.M., Istanbulluoglu, E., and Tucker, G.E., 2017, Creative computing with Landlab: An open-source toolkit for building, coupling, and exploring two-dimensional numerical models of Earth-surface dynamics: Earth Surface Dynamics, v. 5, p. 21–46, https://doi.org/10.5194/esurf-5-21-2017.

Howard, A.D., 1998, Long profile development of bedrock channels: Interaction of weathering, mass wasting, bed erosion, and sediment transport, *in* Tinkler, K.J., and Wohl, E.E., eds., Rivers Over Rock: Fluvial Processes in Bedrock Channels: American Geophysical Union Geophysical Monograph 107, p. 297–319, https://doi.org/10.1029/GM107p0297.

Howard, A.D., 2007, Simulating the development of Martian highland landscapes through the interaction of impact cratering, fluvial erosion, and variable hydrologic forcing: Geomorphology, v. 91, p. 332–363, https://doi.org/10.1016/j.geomorph.2007.04.017.

Hsu, L., Dietrich, W.E., and Sklar, L.S., 2008, Experimental study of bedrock erosion by granular flows: Journal of Geophysical Research: Earth Surface, v. 113, F02001, https://doi.org/10.1029/2007JF000778.

Hughes, M.N., Arvidson, R.E., Grant, J.A., Wilson, S.A., Howard, A.D., and Golombek, M.P., 2019, Degradation of Endeavour Crater based on orbital and rover-based observations in combination with landscape evolution modeling: Journal of Geophysical Research: Planets, v. 124, p. 1472–1494, https://doi.org/10.1029/2019JE005949.

Kokelaar, B.P., Bahia, R.S., Joy, K.H., Viroulet, S., and Gray, J.M.N.T., 2017, Granular avalanches on the Moon: Mass-wasting conditions, processes, and features: Journal of Geophysical Research: Planets, v. 122, p. 1893–1925, https://doi.org/10.1002/2017JE005320.

Kumar, P.S., Head, J.W., and Kring, D.A., 2010, Erosional modification and gully formation at Meteor Crater, Arizona: Insights into crater degradation processes on Mars: Icarus, v. 208, p. 608–620, https://doi.org/10.1016/j.icarus.2010.03.032.

Levin, J.N., Dickson, J.L., and Lamb, M.P., 2022, Evaluating the role of volatiles in bedrock chute formation on the Moon and Mars: Icarus, v. 373, https://doi.org/10.1016/j.icarus.2021.114774.

Malin, M.C., and Edgett, K.S., 2000, Evidence for recent groundwater seepage and surface runoff on Mars: Science, v. 288, p. 2330–2335, https://doi.org/10.1126/science.288.5475.2330.

Malliband, C.C., Conway, S.J., Rothery, D.A., and Balme, M.R., 2019, Potential identification of downslope mass movements on Mercury driven by volatile-loss, *in* 50th Lunar and Planetary Science Conference: Lunar and Planetary Institute Contribution 2132, https://hal.science/hal-02407609 (accessed February 2024).

Perron, J.T., Dietrich, W.E., and Kirchner, J.W., 2008, Controls on the spacing of first-order valleys: Journal of Geophysical Research: Earth Surface, v. 113, https://doi.org/10.1029/2007JF000977.

Pilorget, C., and Forget, F., 2016, Formation of gullies on Mars by debris flows triggered by CO_2 sublimation: Nature Geoscience, v. 9, p. 65–69, https://doi.org/10.1038/ngeo2619.

Ruj, T., Komatsu, G., Kawai, K., Okuda, H., Xiao, Z., and Dhingra, D., 2022, Recent boulder falls within the Finsen crater on the lunar far side: An assessment of the possible triggering rationale: Icarus, v. 377, https://doi.org/10.1016/j.icarus.2022.114904.

Salese, F., Pondrelli, M., Neeseman, A., Schmidt, G., and Ori, G.G., 2019, Geological evidence of planet-wide groundwater system on Mars: Journal of Geophysical Research: Planets, v. 124, p. 374–395, https://doi.org/10.1029/2018JE005802.

Savage, S.B., 1979, Gravity flow of cohesionless granular materials in chutes and channels: Journal of Fluid Mechanics, v. 92, p. 53–96, https://doi.org/10.1017/S0022112079000525.

Sun, Z., Ulizio, T.P., Fischer, J.N., Levin, J.N., Beer, A.R., Dickson, J.L., and Lamb, M.P., 2022, Formation of low-gradient bedrock chutes by dry rockfall on planetary surfaces: Geology, v. 50, p. 174–178, https://doi.org/10.1130/G49286.1.

Vijayan, S., Harish, Kimi, K.B., Tuhi, S., Vigneshwaran, K., Sinha, R.K., Conway, S.J., Sivaraman, B., and Bhardwaj, A., 2022, Boulder Fall Ejecta: Present Day Activity on Mars: Geophysical Research Letters, v. 49, https://doi.org/10.1029/2021GL096808.

Printed in the USA